Cooperative Quantum Optical Effects of Moiré Exciton Superlattices

Haowei Xu,[1,*] Wang Yao,[2] and Ju Li[3,4]
[1]Department of Physics, City University of Hong Kong, Kowloon, Hong Kong SAR, China
[2]New Cornerstone Science Laboratory, Department of Physics, The University of Hong Kong, Hong Kong, China
[3]Department of Nuclear Science and Engineering, Massachusetts Institute of Technology, Cambridge, Massachusetts 02139, USA
[4]Department of Materials Science and Engineering, Massachusetts Institute of Technology, Cambridge, Massachusetts 02139, USA

(Received 13 April 2026; accepted 8 September 2026; published 28 September 2026)

The unique properties of two-dimensional moiré systems have been widely studied from many perspectives. However, relatively little work has investigated how the *real-space* structure of moiré systems can directly engender novel properties and functionalities. In this Letter, we explore how intriguing cooperative optical effects can emerge from the real-space superlattice formed by moiré excitons. Particularly, we show that the collective moiré exciton states can have either strongly enhanced (superradiant) or suppressed (subradiant) radiative decay rates, depending on their in-plane wave vector. These super- and subradiant states can be efficiently switched by a gate-induced electric field gradient. Moreover, the cooperative transmittance T of the atomically thin moiré system can be switched from $T \approx 0$ (opaque) to $T \approx 1$ (transparent) with $\lesssim 1\%$ heterostrain or a 1° adjustment in the twist angle θ. These features are robust against nonradiative losses and disorders, making the moiré system a highly versatile platform for cooperative quantum optics with potential applications in, e.g., single photon storage and switching.

DOI: 10.1103/sp3h-pkqx

Introduction—When two-dimensional materials are stacked with a small twist angle and/or lattice mismatch, the moiré pattern is formed, which exhibits a wide variety of exotic phenomena, such as correlated insulating states, unconventional superconductivity [1,2], and orbital ferromagnetism [3–5]. The photonic and optoelectronic properties of moiré systems [6,7], especially those involving moiré excitons [8–10], have also garnered considerable interest [6,7] with implications for in tunable quantum emitters [6,11], infrared detectors [12], topological excitons [13], etc.

Most previous studies on optical responses have focused on the properties derived from a *single* localized moiré exciton. In reality, however, moiré excitons form a superlattice. One might argue that the total optical response of the superlattice is a simple summation of the responses from each moiré exciton. This viewpoint aligns with conventional treatments of optical responses in condensed-matter systems, where one usually defines a susceptibility ξ per unit cell. The total response is then taken as $N\xi$ with N the number of unit cells participating in the light-matter interaction. This approach is generally valid provided that the phase-matching condition of different light beams is properly included [14]. Within such a framework, the real-space structure of the system enters only through the overall scaling factor N, consistent with the common view that reciprocal k-space structure plays a more central role than real-space structure in condensed-matter physics.

Nevertheless, such a treatment may *not* be adequate for moiré excitons. While the real-space structure of moiré systems is relatively simple (e.g., honeycomblike), few studies have examined how this structure can have *direct* consequences for their properties [15,16]. Crucially, for optical responses, the moiré superlattice constant a_M (10–100 nm when the twist angle is $\theta \lesssim 1°$) can become a considerable fraction of the resonant wavelength λ_0 (hundreds of nanometers). In this regime, moiré excitons can interfere constructively or destructively during light-matter interactions, so their real-space structure may fundamentally reshape the overall optical response, which can be far from the simple summation $N\xi$.

The discussions above motivate us to investigate the *cooperative* optical response of the moiré exciton superlattices. Cooperative optical effects, such as collective Lamb shift [17] and the subradiant optical mirror effect [18], have primarily been explored in, e.g., artificial atom arrays [19–21], but have rarely been studied in intrinsic condensed-matter systems. While isolated atoms benefit from narrow nonradiative linewidths, it is experimentally challenging to assemble large and perfectly ordered atomic arrays, limiting their practical applicability. In contrast, moiré systems naturally form ordered lattices with unit filling; that is, each lattice site hosts one exciton. This is an arrangement that is difficult to realize in artificial atomic platforms. Moreover, the moiré superlattice constant a_M and many other properties can be conveniently controlled by the twist angle θ and heterostrain. These features make moiré systems highly promising platforms for exploring

*Contact author: haoweixu@cityu.edu.hk

 © 2026 American Physical Society

cooperative quantum optical phenomena and their potential applications.

In the following, we begin by introducing the properties of moiré excitons and show that each exciton can be modeled as a two-level system with an optical transition dipole. We then explore several significant cooperative quantum optical effects of moiré exciton superlattices. Particularly, we show that collective moiré exciton states can have extremely high (superradiant) or low (subradiant) radiative decay rates, depending on their in-plane wave vector. The subradiant states can have lifetimes extended by orders of magnitude compared with that of a single exciton, making them promising candidates for photon memory [22,23]. Additionally, a gate-induced electric field gradient can dynamically switch the system between superradiant and subradiant states, enabling efficient photon storage and retrieval. We further demonstrate that though the moiré system is atomically thin, its light transmittance T can be tuned from $T \approx 1$ to $T \approx 0$, with less than 2% heterostrain or 1° change in the twist angle, allowing the system to function as an efficient single photon switch [24]. These properties remain robust against nonradiative losses and inhomogeneous broadening up to a few hundred GHz, well within experimental reach, given that the overall linewidth of moiré excitons can be as narrow as 20 GHz [9].

Properties of moiré excitons—We first introduce the properties of single moiré excitons, focusing on their spatial localization and optical transitions. We will show that the moiré exciton on each superlattice site can be modeled as a two-level system with ground state $|G\rangle$, excited state $|R\rangle$, and transition dipole moment d (Fig. 2). Detailed discussions can be found in Secs. 1–4 of the Supplemental Material [25].

Without the moiré potential, a free exciton state can be labeled by $|Q\rangle$, with total momentum Q and total energy $\hbar\omega_0 + \hbar^2 Q^2/2M$. Here, $\hbar\omega_0$ is the energy of a zero-momentum exciton, typically on the order of 1 eV [35]. Meanwhile, $(\hbar^2 Q^2/2M)$ is the kinetic energy of the exciton with M the total mass of the electron and hole. Notably, $|Q\rangle$ are delocalized plane-wave-like states, and the exciton center-of-mass coordinate r has a simple spatial profile $Q(r) \sim e^{iQ\cdot r}$. The optical transition dipole between the ground state $|G\rangle$ (i.e., no exciton) and $|Q\rangle$ is nonzero only when $Q = q_{i=1,2,3}$, where $q_1 = K_T - K_B$, while q_2 and q_3 are obtained from q_1 by $2\pi/3$ and $4\pi/3$ rotations, respectively. Here K_T and K_B are the K valleys of the top and bottom layers [Fig. 1(b) and Fig. S2 in Ref. [25]]. This is because the photon momentum is negligible, so an electron at K_B would acquire a wave vector of q_i relative to K_T after a vertical optical transition [Fig. 1(b)]. The optically bright momenta $Q = q_1, q_2, q_3$ are equivalent due to the threefold rotational symmetry of the system.

The moiré structure leads to a potential field $\Delta(r)$ for the excitons, which has the same periodicity as the moiré supercell [Fig. 1(a)]. This is because at different locations of the moiré supercell, the upper and lower layers have

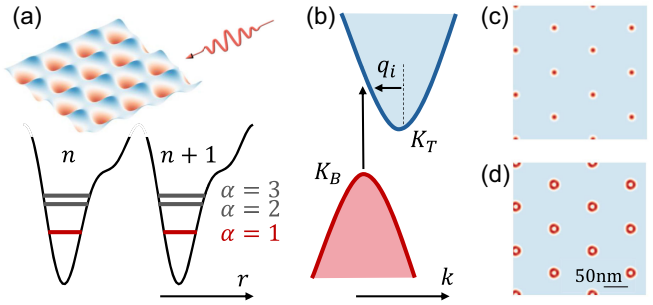


FIG. 1. (a) Illustrations of moiré potential and exciton lattice in real space. The upper panel shows a two-dimensional moiré potential landscape. The lower panel shows multiple localized moiré exciton states in each potential minimum, labeled by α. We focus on the lowest energy $\alpha = 1$ state. (b) Illustration of the electronic band structure of the moiré system in the unfolded Brillouin zone. The electron acquires a wave vector q_i relative to K_T after a vertical optical transition from K_B. There are three symmetry-equivalent $q_{i=1,2,3}$, related by $2\pi/3$ rotations. (c),(d) Real space wave function $|\langle r|\chi_\alpha\rangle|$ of (c) $\alpha = 1$ and (d) $\alpha = 2$ exciton with $\theta = 0.2°$. Blue (red) color denotes small (large) wave function amplitude.

different stacking patterns, resulting in different local environments. The potential $\Delta(r)$ results in the hybridization between free exciton states, namely, $\langle Q|\Delta(r)|Q'\rangle = \sum_{n=1}^{6} V_n \delta_{Q,Q'+b_n}$, where δ is the Kronecker delta, b_n are the moiré reciprocal lattice vectors, and V_n characterizes the depth of the moiré potential, which is typically tens of meV for interlayer excitons [11,13].

The new moiré exciton eigenstates are $|\chi_{\alpha,Q}\rangle = \sum_{Q'} f^{\alpha}_{QQ'}|Q'\rangle$, where $f^{\alpha}_{QQ'}$ is the wave function. Here, Q is restricted to the first moiré Brillouin zone, while other Q points outside the first moiré Brillouin zone are folded back into it, giving rise to an additional band index α. The energy difference between different α states is on the order of meV (Fig. 1(a), and Sec. 2 in Ref. [25]). This is analogous to the formation of electron bands in the nearly free electron model [36]. We focus on the lowest-energy $\alpha = 1$ mode that is optically bright. The influence of other modes is discussed in Sec. 4.2 in Ref. [25]. Due to the hybridization induced by $\Delta(r)$, the optically bright moiré exciton eigenstates contain equivalent contributions from $Q = q_1, q_2, q_3$ modes, resulting in a total momentum of zero (since $q_1 + q_2 + q_3 = 0$). In the following, we will use the shorthand $|\chi\rangle$ to denote this particular mode unless otherwise noted.

Next, we consider the spatial profile of the moiré exciton. The real-space wave function, expressed as $\langle r|\chi\rangle = \sum_{Q'} f_{QQ'} e^{iQ'\cdot r}$, is localized at the minima of the moiré potential [Figs. 1(c) and 1(d)]. One can define approximate exciton wave packets $|R\rangle = \sum_{Q'} W(Q')|Q'\rangle$, mimic an exciton localized at the lattice site R with a proper choice of $W(Q')$. Notably, the width w of the moiré exciton wave function is on the order of a few nanometers, much smaller than the optical wavelength, which is hundreds of nanometers. Therefore, each localized moiré exciton can be

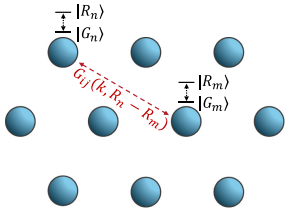


FIG. 2. An ordered moiré superlattice. Each lattice site R_n is modeled by a two-level system $|R_n\rangle$ and $|G_n\rangle$ with transition dipole d. The red arrow indicates the electromagnetic interactions among moiré excitons, characterized by the Green's function G_{ij}.

treated as a pointlike dipole in optical response calculations. This significantly simplifies the analyses of their cooperative optical response.

The width of the wave packet w is also crucial in the optical transitions. Particularly, the optical transition dipole moment $d \equiv \langle G|\hat{d}|R\rangle$ is proportional to w. Here $\hat{d}$ is the dipole operator and $|G\rangle$ is the ground state; i.e., there are no excitons at this lattice point. The property of $d \propto w$ is similar to the optical transition dipoles of quantum dots, which scale linearly with their size [37]. For a wide range of twist angles, one has $w \sim 0.3a_M \propto 1/\theta$. Hence, we adopt $d \approx d_0/\theta$ with $d_0 = 0.1\ e \cdot$ Å. As d increases for larger a_M (smaller θ), the dipole-dipole interaction among moiré excitons can remain strong even if a_M is large (Sec. 2 in Ref. [25]).

Strictly speaking, excitons are bosons, so multiple excitons can, in principle, occupy the same potential minimum. However, if more than one exciton occupies the same site, then the on-site exciton-exciton interactions would introduce a resonance frequency shift [11] (analogous to the Hubbard U for electrons), much larger than the energy scale relevant here. Hence, when the incident light is (nearly) resonant with the transition between $|G\rangle$ (no exciton) and $|R\rangle$ (one exciton), states with multiple excitons are far off resonance and can be neglected. In Sec. 4 in Ref. [25], we systematically analyze the validity of using the two-level system approximation for the moiré exciton superlattice.

Interactions among moiré excitons—In the previous section, we focused on the properties of a single moiré exciton. Now we turn to the ordered superlattice formed by N moiré excitons. We will use a subscript n to denote an exciton at lattice site R_n. Each lattice site R_n is thus modeled by a two-level system $|R_n\rangle$ and $|G_n\rangle$ with transition dipole d (Fig. 2).

These localized moiré excitons interact with one another through dipole-dipole interactions. For two excitons at locations R_n and R_m, one has the Green's function as

$$G_{ij}(k,r) = \frac{e^{ikr}}{4\pi k^2 r^3}\left[(k^2r^2 + ikr - 1)\delta_{ij} + (-k^2r^2 - 3ikr + 3)\frac{r_i r_j}{r^2}\right]. \quad (1)$$

Here k is the wave vector of the electromagnetic field. We define $r = R_n - R_m$. i, j are Cartesian indices, and δ_{ij} is the Kronecker delta. The vacuum Green's function [38] is used here for simplicity. The influence of the dielectric environment arising from, for example, the substrate and encapsulation layers, is discussed in Sec. 8 in Ref. [25].

The interactions among dipoles, encoded in the Green's function, can lead to exotic cooperative effects, as we will discuss below.

Superradiant and subradiant states—We will first discuss super- and subradiance of the collective moiré exciton states [20,39,40], and how they can be dynamically switched, providing a mechanism for light storage and retrieval.

The total Hamiltonian of the exciton lattice is [20]

$$H_{\text{eff}} = \hbar\omega_0 \sum_{n=1}^{N} |R_n\rangle\langle R_n| + \frac{k_0^2 d^2}{\varepsilon_0} \times \sum_{m,n} G_{xx}(k_0, R_n - R_m)|G_n\rangle|R_m\rangle\langle R_n|\langle G_m|. \quad (2)$$

The first term is the noninteracting Hamiltonian, which is zero ($\hbar\omega_0$) if a lattice site is on $|G_n\rangle$ (on $|R_n\rangle$). The second term describes the long-range dipole-dipole interaction among moiré excitons. Here, ε_0 is vacuum permittivity, and we define $k_0 = \omega_0/c_0$ with c_0 the speed of light. The transition dipole d is assumed to be the same for all excitons. This term accounts for Forster-type nonradiative coupling that allows moiré excitons to effectively hop between the trapping sites [16]. We did not include the out-of-plane permanent dipole $d_z \equiv \langle R_n|\hat{d}|R_n\rangle$ of the interlayer exciton, as it is much smaller than d [11]. Without loss of generality, we consider excitons excited by light polarized along the x direction, so only G_{xx} appears in Eq. (2). The full H_{eff} has a dimension of 2^N, but we focus on the single-excitation subspace spanned by the basis $|\psi^n\rangle \equiv |G_1G_2,\ldots,R_n,\ldots,G_N\rangle, n = 1,2,\ldots,N$, whose dimension is N. The validity of using only the single-excitation subspace will be discussed in Sec. 4 in Ref. [25]. In essence, in terms of the interaction described in Eq. (2), including the double- and higher-excitation states would not affect the properties within the single-excitation subspace.

The effective Hamiltonian H_{eff} is non-Hermitian. Nevertheless, one can still investigate its eigenstates $|\nu\rangle$ with complex eigenvalues $J_\nu - i\Gamma_\nu/2$. Here, J_ν and Γ_ν correspond to the collective line shift and radiative decay rate, respectively. Generally, $|\nu\rangle$ are collective exciton states, similar to the Bloch functions, and $|\langle\psi_n|\nu\rangle|^2$ is the probability of finding the exciton at lattice site R_n.

For an infinite exciton lattice, $|\nu\rangle$ can be labeled by the in-plane wave vector $k_\parallel$, according to Bloch's theorem. That is, one has $|\nu(k_\parallel)\rangle \propto \sum_n e^{ik_\parallel \cdot R_n}|\psi_n\rangle$. Notably, for $k_\parallel > k_0$, one has $\Gamma_\nu = 0$, and the excitons are completely dark (Sec. 5 in Ref. [25]). For $k_\parallel < k_0$, superradiance $\Gamma_\nu > \gamma_0$ occurs. This superradiance-subradiance transition arises

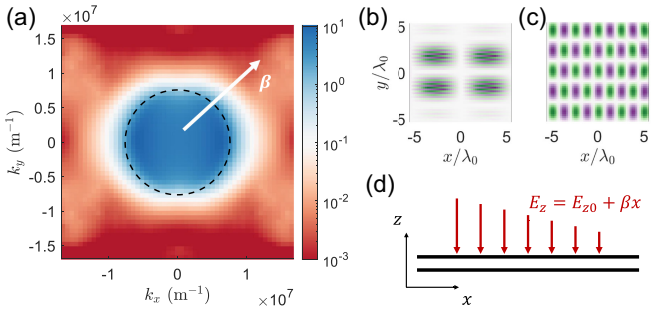


FIG. 3. (a) Collective radiative decay rate Γ_ν as a function of in-plane wave vector $k_\parallel$ for a finite lattice with approximately 50×50 excitons. The dashed circle denotes the light cone with $|k_\parallel| = k_0$. (b),(c) Real part of the wave function of the collective exciton in real space, i.e., $\mathrm{Re}[\langle\psi_n|\nu(k_\parallel)\rangle]$. Panels (b) and (c) correspond to two states with $|k_\parallel| > k_0$ and $|k_\parallel| < k_0$, respectively. Each pixel corresponds to a moiré lattice site R_n. Blue (purple) color indicates positive (negative) values of the wave function. (d) A collective exciton state can be switched between superradiant and subradiant states by an electric field gradient β. The electric field is along the out-of-plane z direction, while the gradient is along the in-plane x or y direction.

from momentum conservation: the in-plane momentum $k_\parallel$ of the emitted photon must match that of the collective exciton. For $k_\parallel > k_0$, the out-of-plane wave vector $\sqrt{k_0^2 - k_\parallel^2}$ becomes imaginary, producing an evanescent field and suppressing radiation ($\Gamma_\nu = 0$).

In practice, the moiré exciton lattice is finite, and one cannot assign a definite $k_\parallel$ to each eigenstate. In this regard, we numerically diagonalize H_{eff} for a $N = 2874 \approx 50 \times 50$ exciton lattice, and selected wave functions $|\nu\rangle$ are plotted in Figs. 3(b) and 3(c). These states exhibit semiperiodic patterns, allowing for a Fourier transform to extract the dominant $k_\parallel$ component, which can be used to label $|\nu\rangle$ as $\langle\psi_n|\nu(k_\parallel)\rangle \approx e^{ik_\parallel \cdot R_n}$. Using this approach, we obtained the Γ_ν-$k_\parallel$ relationship [Fig. 3(a)] for a finite lattice. Notably, there is still a transition from superradiance ($\Gamma_\nu \gg \gamma_0$) to subradiance ($\Gamma_\nu \ll \gamma_0$) at the light cone boundary $|k_\parallel| = k_0$. The transition is smooth due to the finite-size effect, and states with $|k_\parallel| > k_0$ are not entirely dark—their Γ_ν is small but nonzero. Here, the 50×50 lattice has a spatial size of about 10 μm × 10 μm. This system size is chosen for two main reasons: (1) it is already significantly larger than the wavelength of the resonant light ($\lesssim$1 μm), ensuring that collective effects are well developed; (2) experimentally, fabricating substantially larger high-quality moiré samples may be challenging. It should be noted that the contrast between superradiant and subradiant states is stronger for larger lattice size, and becomes strongest for an infinite lattice, as shown in Sec. 5.3 in Ref. [25].

Switching between superradiant and subradiant states—A collective exciton state excited by an external photon must have $k_\parallel < k_0$ and is therefore superradiant. This allows the photon to be efficiently transferred into an exciton state. For long-term photon storage, however, the excitation should reside in a subradiant state, which has a much longer lifetime.

Hence, effective light storage and retrieval require controllable switching between superradiant and subradiant states. This can be achieved by applying a gate electric field with a spatial gradient, which leads to a Hamiltonian $H_\beta = \sum_n d_z \cdot \beta \cdot R_n |R_n\rangle\langle R_n|$, where $d_z = \langle R_n|\hat{d}|R_n\rangle$ is the out-of-plane dipole of the exciton. This electric field is along the z direction, while the gradient β lies in plane [along x or y in Fig. 3(d)]. H_β induces a position-dependent phase, effectively shifting the exciton wave vector, namely [41],

$$k_\parallel \to k_\parallel + \frac{d_z \cdot \beta}{\hbar}\tau, \tag{3}$$

with τ the duration of the applied electric field gradient. With a suitable τ, a superradiant exciton can be pushed beyond the light cone and become subradiant. In practice, this can be achieved within nanoseconds with $\beta \sim 10^{10}$ V/m^2. To restore the superradiant state, one can simply reverse the direction of the electric field ($-\beta$) for the same duration τ. Note that β does not need to be uniform in real space.

Intuitively, Eq. (3) resembles the semiclassical equation of motion for an electron in a crystal, $k \to k + eE\tau/\hbar$, where the electron charge e couples directly to the electric field E. In contrast, an exciton carries no net charge but only a dipole moment d_z, so its wave vector can be modified only via the electric-field gradient β.

Cooperative photon scattering—Besides photon absorption and emission, cooperative optical effects also appear in photon scattering. As an example, we study the transmittance T of the moiré exciton lattice. Typically, few-layer 2D materials have $T \approx 1$, as they are too thin to significantly reflect or absorb light. For example, monolayer graphene has $T \approx 0.97$ [42]. Remarkably, as we show below, the moiré exciton lattice can exhibit nearly zero transmittance.

Assuming an incident field $E_0(r)$ with frequency ω and wavelength λ, the total field $E(r)$ after scattering with the excitons should satisfy [19,21,34]

$$E_i(r) = E_{0,i}(r) + \frac{4\pi^2\alpha}{\varepsilon_0\lambda^2}\sum_{jn} G_{ij}(k, r - R_n)E_j(R_n). \tag{4}$$

For simplicity, we consider x-polarized light incident normally along z onto the exciton lattice plane (x-y plane). Other geometries can be analyzed similarly. Equation (4) indicates that the total field $E(r)$ is the sum of the incident field $E_0(r)$ and the field scattered by the exciton dipole at R_n, mediated by the propagator $G_{ij}(k, r - R_n)$. The exciton polarizability is $\alpha(\omega) = (2d^2\omega_0/\hbar)[1/(\omega_0^2 - \omega^2 - i\gamma\omega)]$. The total linewidth of a single exciton is given by $\gamma = \gamma_r + \gamma_{\mathrm{nr}}$, where γ_r and γ_{nr} are the radiative and nonradiative components, respectively. Each moiré exciton

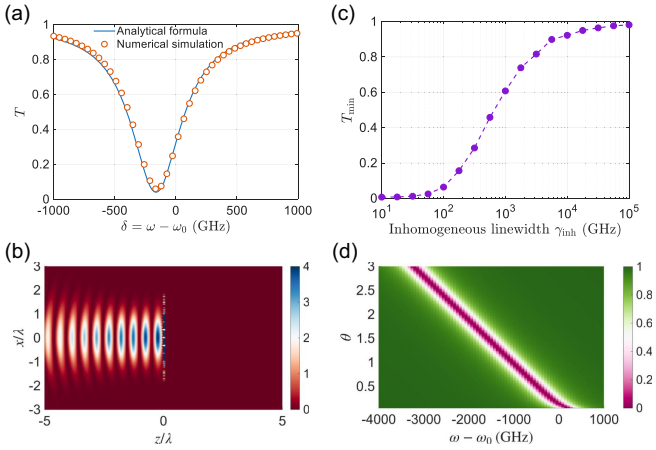


FIG. 4. (a) Transmittance $T(\omega)$ as a function of frequency detuning $\omega-\omega_0$ with $\theta=0.2°$. (b) The electric field profile $|E(r)|^2$ at $\omega-\omega_0\approx-161$ GHz, where $T(\omega)$ reaches the minimum at $\theta=0.2°$. Light is incident from the left, and the fields $|E(r)|^2$ are normalized by E_0^2 with E_0 the incident field strength. (c) Minimum of T as a function of inhomogeneous linewidth with $\theta=0.2°$. (d) T as a function of $\omega-\omega_0$ for varied θ. The nonradiative linewidth is taken as $\gamma_{\rm nr}=100$ GHz.

may also experience an inhomogeneous shift in its resonance frequency ω_0, characterized by an inhomogeneous linewidth $\gamma_{\rm inh}$.

We first numerically study a finite exciton lattice with $\theta=0.2°$ ($a_M\approx0.11\lambda_0$) with $\gamma_{\rm nr}=100$ GHz and $\gamma_{\rm inh}=0$ (details in Sec. 6 in Ref. [25]). The transmittance T versus frequency detuning $\delta=\omega-\omega_0$ is plotted in Fig. 4(a). Intriguingly, nearly zero transmission appears at $\delta\approx-161$ GHz. The field profile [Fig. 4(b)] shows that the scattered field and the incident field form a standing wave in the $z<0$ region. In the $z>0$ region, the two fields add destructively, leading to zero transmission (Sec. 6.1 in Ref. [25]).

Analytically, for an infinite exciton lattice with $a_M<\lambda$, one has (Sec. 6.2 in Ref. [25])

$$T(\omega)=\left|1-\frac{\frac{i}{2}\left(\frac{\lambda_0^3}{\lambda^3}\gamma_0+\Gamma\right)}{\omega-\omega_0+\Delta+\frac{i}{2}(\gamma_0+\gamma_{\rm nr}+\Gamma)}\right|^2, \quad (5)$$

where the collective lineshift Δ and the collective radiative decay rate Γ are

$$\Delta=\frac{3\gamma_0}{2}\frac{\lambda_0^3}{\lambda^3}\lambda{\rm Re}\{\mathcal{G}_{xx}(0)\},\qquad \Gamma=\frac{3\gamma_0}{4\pi}\frac{\lambda_0^3}{\lambda^3}\frac{\lambda^2}{A}-\frac{\lambda_0^3}{\lambda^3}\gamma_0, \quad (6)$$

with $\mathcal{G}_{xx}(0)=\sum_{n\neq0}G_{xx}(k,R_n)$ and A the area of the moiré superlattice unit cell. Intuitively, the moiré excitons interact cooperatively [Eq. (1) and Fig. 2], forming a collective excitation that behaves like a giant atom. Zero transmittance occurs at the collective resonance $\Delta+\omega-\omega_0=0$ when $\gamma_{\rm nr}=0$, which is demonstrated in Fig. 4(d) for varied θ.

Notably, this cooperative effect is robust to inhomogeneity $\gamma_{\rm inh}$ and nonradiative damping $\gamma_{\rm nr}$, provided that they remain below the *collective* radiative decay rate Γ in Eq. (5). Our results indicate that transmittance below 0.2 can be realized with $\gamma_{\rm inh},\gamma_{\rm nr}\lesssim100$ GHz [Fig. 4(c) and Sec. 6.3 in Ref. [25]].

More importantly, this effect is highly sensitive to the real space structure of the moiré exciton superlattice, enabling an efficient light switch. At a fixed light frequency, nearly zero transmission $T\approx0$ and full transmission $T\approx1$ can be toggled by varying the twist angle θ by less than 1° [Fig. 4(d)]. This is because the collective shift Δ strongly depends on the moiré lattice spacing, which is controlled by the twist angle. From this perspective, a heterostrain u can also be used to tune T. This is because applying heterostrain is effectively equivalent to tuning θ in terms of modifying the lattice constant $a_M\propto1/\sqrt{u^2+\theta^2}$. Using heterostrain $u\lesssim1\%$, one can realize *in situ* and reversible control over T.

Discussions—It is well-known that the optical response of an atom is strongly influenced by its electromagnetic environment. For example, an optical cavity can modify the atomic radiative decay through the Purcell effect [43], and single photon switching can be achieved with atoms in nanophotonic platforms [44,45]. From this perspective, in a moiré exciton lattice, the local electromagnetic environment experienced by each exciton is set by its neighboring excitons. An exciton A can (virtually) transfer its excitation to surrounding excitons and receive it back [16], meaning that neighboring excitons effectively act as a resonator for exciton A [46]. In this sense, the moiré exciton lattice parallels a single atom coupled to a nanophotonic structure, thereby enabling the cooperative quantum optical functionalities discussed above.

The cooperative optical effects of the moiré excitons are robust against positional disorder, vacancies of localized moiré excitons, and variations in the magnitude of transition dipoles, but are more sensitive to inhomogeneity in exciton resonance frequencies $\delta\omega_0$. The system can tolerate $\delta\omega_0$ on the order of a few hundred GHz (details in Sec. 7 in Ref. [25]). Fortunately, linewidths down to tens of GHz have been reported at a few Kelvin [9]. In non-moiré two-dimensional materials, exciton lifetimes can even reach the microsecond range [47], and the cooperative coupling and superradiance of excitons have been experimentally observed [48,49]. Therefore, cooperative quantum optics with moiré exciton superlattices, as proposed here, should be experimentally feasible with high-quality, low-disorder samples. The moiré superlattice thus provides a versatile platform for exploring both fundamental cooperative many-body quantum optics and their potential applications, all in the two-dimensional limit.

Acknowledgments—H. X. acknowledges the support from the startup funding from City University of Hong Kong.

Data availability—The data are available from the authors upon reasonable request.

[1] Yuan Cao, Valla Fatemi, Shiang Fang, Kenji Watanabe, Takashi Taniguchi, Efthimios Kaxiras, and Pablo Jarillo-Herrero, Unconventional superconductivity in magic-angle graphene superlattices, Nature (London) **556**, 43 (2018).

[2] Yuan Cao, Valla Fatemi, Ahmet Demir, Shiang Fang, Spencer L Tomarken, Jason Y Luo, Javier D Sanchez-Yamagishi, Kenji Watanabe, Takashi Taniguchi, Efthimios Kaxiras *et al.*, Correlated insulator behaviour at half-filling in magic-angle graphene superlattices, Nature (London) **556**, 80 (2018).

[3] Aaron L. Sharpe, Eli J. Fox, Arthur W. Barnard, Joe Finney, Kenji Watanabe, Takashi Taniguchi, M. A. Kastner, and David Goldhaber-Gordon, Emergent ferromagnetism near three-quarters filling in twisted bilayer graphene, Science **365**, 605 (2019).

[4] Guorui Chen, Aaron L. Sharpe, Eli J. Fox, Ya-Hui Zhang, Shaoxin Wang, Lili Jiang, Bosai Lyu, Hongyuan Li, Kenji Watanabe, Takashi Taniguchi *et al.*, Tunable correlated Chern insulator and ferromagnetism in a moiré superlattice, Nature (London) **579**, 56 (2020).

[5] M. Serlin, C. L. Tschirhart, H. Polshyn, Y. Zhang, J. Zhu, K. Watanabe, T. Taniguchi, L. Balents, and A. F. Young, Intrinsic quantized anomalous Hall effect in a moiré heterostructure, Science **367**, 900 (2020).

[6] Hyeonjun Baek, Mauro Brotons-Gisbert, Zhe Xian Koong, Aidan Campbell, Markus Rambach, Kenji Watanabe, Takashi Taniguchi, and Brian D. Gerardot, Highly energy-tunable quantum light from moiré-trapped excitons, Sci. Adv. **6**, eaba8526 (2020).

[7] Luojun Du, Maciej R. Molas, Zhiheng Huang, Guangyu Zhang, Feng Wang, and Zhipei Sun, Moiré photonics and optoelectronics, Science **379**, eadg0014 (2023).

[8] Kha Tran, Galan Moody, Fengcheng Wu, Xiaobo Lu, Junho Choi, Kyounghwan Kim, Amritesh Rai, Daniel A. Sanchez, Jiamin Quan, Akshay Singh *et al.*, Evidence for moiré excitons in van der Waals heterostructures, Nature (London) **567**, 71 (2019).

[9] Kyle L. Seyler, Pasqual Rivera, Hongyi Yu, Nathan P. Wilson, Essance L. Ray, David G. Mandrus, Jiaqiang Yan, Wang Yao, and Xiaodong Xu, Signatures of moiré-trapped valley excitons in MoSe2/WSe2 heterobilayers, Nature (London) **567**, 66 (2019).

[10] Chenhao Jin, Emma C. Regan, Aiming Yan, M. Iqbal Bakti Utama, Danqing Wang, Sihan Zhao, Ying Qin, Sijie Yang, Zhiren Zheng, Shenyang Shi *et al.*, Observation of moiré excitons in WSe2/WS2 heterostructure superlattices, Nature (London) **567**, 76 (2019).

[11] Hongyi Yu, Gui-Bin Liu, Jianju Tang, Xiaodong Xu, and Wang Yao, Moiré excitons: From programmable quantum emitter arrays to spin-orbit–coupled artificial lattices, Sci. Adv. **3**, e1701696 (2017).

[12] Chao Ma, Shaofan Yuan, Patrick Cheung, Kenji Watanabe, Takashi Taniguchi, Fan Zhang, and Fengnian Xia, Intelligent infrared sensing enabled by tunable moiré quantum geometry, Nature (London) **604**, 266 (2022).

[13] F. Wu, T. Lovorn, and A. H. MacDonald, Topological exciton bands in moiré heterojunctions, Phys. Rev. Lett. **118**, 147401 (2017).

[14] Yuen-Ron Shen, *The Principles of Nonlinear Optics* (1983).

[15] Haochen Wang and Wang Yao, Emergent Kagome lattice and non-Abelian lattice gauge field of biexcitons in t-MoTe2, Nat. Sci. Rev. **13**, nwaf328 (2026).

[16] Huiyuan Zheng, Ci Li, Hongyi Yu, and Wang Yao, Förster valley-orbit coupling and topological lattice of hybrid moiré excitons, Commun. Phys. **8**, 193 (2025).

[17] Antoine Glicenstein, Giovanni Ferioli, Nikola Šibalić, Ludovic Brossard, Igor Ferrier-Barbut, and Antoine Browaeys, Collective shift in resonant light scattering by a one-dimensional atomic chain, Phys. Rev. Lett. **124**, 253602 (2020).

[18] Jun Rui, David Wei, Antonio Rubio-Abadal, Simon Hollerith, Johannes Zeiher, Dan M Stamper-Kurn, Christian Gross, and Immanuel Bloch, A subradiant optical mirror formed by a single structured atomic layer, Nature (London) **583**, 369 (2020).

[19] Robert J. Bettles, Simon A. Gardiner, and Charles S. Adams, Enhanced optical cross section via collective coupling of atomic dipoles in a 2D array, Phys. Rev. Lett. **116**, 103602 (2016).

[20] A. Asenjo-Garcia, M. Moreno-Cardoner, A. Albrecht, H. J. Kimble, and D. E. Chang, Exponential improvement in photon storage fidelities using subradiance and selective radiance in atomic arrays, Phys. Rev. X **7**, 031024 (2017).

[21] Ephraim Shahmoon, Dominik S. Wild, Mikhail D. Lukin, and Susanne F. Yelin, Cooperative resonances in light scattering from two-dimensional atomic arrays, Phys. Rev. Lett. **118**, 113601 (2017).

[22] Sheng Zhang, Jixuan Shi, Zhaibin Cui, Ye Wang, Yukai Wu, Luming Duan, and Yunfei Pu, Realization of a programmable multipurpose photonic quantum memory with over-thousand qubit manipulations, Phys. Rev. X **14**, 021018 (2024).

[23] Yu-Ping Liu, Zhong-Wen Ou, Tian-Xiang Zhu, Ming-Xu Su, Chao Liu, Yong-Jian Han, Zong-Quan Zhou, Chuan-Feng Li, and Guang-Can Guo, A millisecond integrated quantum memory for photonic qubits, Sci. Adv. **11**, eadu5264 (2025).

[24] Shuo Sun, Hyochul Kim, Zhouchen Luo, Glenn S Solomon, and Edo Waks, A single-photon switch and transistor enabled by a solid-state quantum memory, Science **361**, 57 (2018).

[25] See Supplemental Material at http://link.aps.org/supplemental/10.1103/sp3h-pkqx for detailed discussions on the properties of moiré excitons and their cooperative optical responses; includes Refs. [9,11,20,26–34].

[26] Mads L. Trolle, Gotthard Seifert, and Thomas G. Pedersen, Theory of excitonic second-harmonic generation in monolayer MoS_2, Phys. Rev. B **89**, 235410 (2014).

[27] F. Wu, T. Lovorn, and A. H. MacDonald, Theory of optical absorption by interlayer excitons in transition metal dichalcogenide heterobilayers, Phys. Rev. B **97**, 035306 (2018).

[28] Junyeong Ahn, Guang-Yu Guo, and Naoto Nagaosa, Low-frequency divergence and quantum geometry of the bulk photovoltaic effect in topological semimetals, Phys. Rev. X **10**, 041041 (2020).
[29] Chongyun Jiang, Weigao Xu, Abdullah Rasmita, Zumeng Huang, Ke Li, Qihua Xiong, and Wei-bo Gao, Microsecond dark-exciton valley polarization memory in two-dimensional heterostructures, Nat. Commun. **9**, 753 (2018).
[30] Cédric Robert, Bo Han, Piotr Kapuscinski, Alex Delhomme, Clément Faugeras, Thierry Amand, Maciej R. Molas, Miroslav Bartos, Kenji Watanabe, Takashi Taniguchi *et al.*, Measurement of the spin-forbidden dark excitons in MoS_2 and $MoSe_2$ monolayers, Nat. Commun. **11**, 4037 (2020).
[31] Alireza Taghizadeh and Thomas Garm Pedersen, Gauge invariance of excitonic linear and nonlinear optical response, Phys. Rev. B **97**, 205432 (2018).
[32] Alireza Taghizadeh and Thomas Garm Pedersen, Nonlinear excitonic spin Hall effect in monolayer transition metal dichalcogenides, 2D Mater. **7**, 015003 (2020).
[33] Charalambos Louca, Armando Genco, Salvatore Chiavazzo, Thomas P. Lyons, Sam Randerson, Chiara Trovatello, Peter Claronino, Rahul Jayaprakash, Xuerong Hu, James Howarth *et al.*, Interspecies exciton interactions lead to enhanced nonlinearity of dipolar excitons and polaritons in MoS_2 homobilayers, Nat. Commun. **14**, 3818 (2023).
[34] Francisco Javier Garcia de Abajo, Colloquium: Light scattering by particle and hole arrays, Rev. Mod. Phys. **79**, 1267(C) (2007).
[35] Gang Wang, Alexey Chernikov, Mikhail M. Glazov, Tony F. Heinz, Xavier Marie, Thierry Amand, and Bernhard Urbaszek, Colloquium: Excitons in atomically thin transition metal dichalcogenides, Rev. Mod. Phys. **90**, 021001(C) (2018).
[36] Charles Kittel and Paul McEuen, *Introduction to Solid State Physics* (John Wiley & Sons, New York, 2018).
[37] Lucjan Jacak, Pawel Hawrylak, and Arkadiusz Wojs, *Quantum Dots* (Springer Science & Business Media, New York, 2013).
[38] Lukas Novotny and Bert Hecht, *Principles of Nano-Optics* (Cambridge University Press, Cambridge, England, 2012).
[39] Robert H. Dicke, Coherence in spontaneous radiation processes, Phys. Rev. **93**, 99 (1954).
[40] Stuart J. Masson, Igor Ferrier-Barbut, Luis A. Orozco, Antoine Browaeys, and Ana Asenjo-Garcia, Many-body signatures of collective decay in atomic chains, Phys. Rev. Lett. **125**, 263601 (2020).
[41] David Plankensteiner, Laurin Ostermann, Helmut Ritsch, and Claudiu Genes, Selective protected state preparation of coupled dissipative quantum emitters, Sci. Rep. **5**, 16231 (2015).
[42] Shou-En Zhu, Shengjun Yuan, and GCAM Janssen, Optical transmittance of multilayer graphene, Europhys. Lett. **108**, 17007 (2014).
[43] Edward Mills Purcell, Spontaneous emission probabilities at radio frequencies, in *Confined Electrons and Photons: New Physics and Applications* (Springer, New York, 1995), pp. 839–839.
[44] T. G. Tiecke, Jeffrey Douglas Thompson, Nathalie Pulmones de Leon, L. R. Liu, Vladan Vuletić, and Mikhail D. Lukin, Nanophotonic quantum phase switch with a single atom, Nature (London) **508**, 241 (2014).
[45] Itay Shomroni, Serge Rosenblum, Yulia Lovsky, Orel Bechler, Gabriel Guendelman, and Barak Dayan, All-optical routing of single photons by a one-atom switch controlled by a single photon, Science **345**, 903 (2014).
[46] Raphael Holzinger, David Plankensteiner, Laurin Ostermann, and Helmut Ritsch, Nanoscale coherent light source, Phys. Rev. Lett. **124**, 253603 (2020).
[47] Luis A. Jauregui, Andrew Y. Joe, Kateryna Pistunova, Dominik S. Wild, Alexander A. High, You Zhou, Giovanni Scuri, Kristiaan De Greve, Andrey Sushko, Che-Hang Yu *et al.*, Electrical control of interlayer exciton dynamics in atomically thin heterostructures, Science **366**, 870 (2019).
[48] Jason Horng, Yu-Hsun Chou, Tsu-Chi Chang, Chu-Yuan Hsu, Tien-Chang Lu, and Hui Deng, Engineering radiative coupling of excitons in 2D semiconductors, Optica **6**, 1443 (2019).
[49] Golam Haider, Krishna Sampathkumar, Tim Verhagen, Lukas Nadvornik, Farjana J. Sonia, Václav Valeš, Jan Sýkora, Peter Kapusta, Petr Němec, Martin Hof *et al.*, Superradiant emission from coherent excitons in van der Waals heterostructures, Adv. Funct. Mater. **31**, 2102196 (2021).